Detailed-balance assessment of radiative cooling for multi-junction solar cells under unconcentrated and low-concentrated light

Solar Energy Materials & Solar Cells 274 (2024) 112958

Contents lists available at ScienceDirect

Solar Energy Materials and Solar Cells

journal homepage: www.elsevier.com/locate/solmat

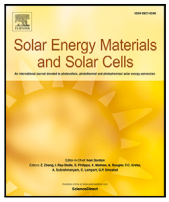

Detailed-balance assessment of radiative cooling for multi-junction solar cells under unconcentrated and low-concentrated light

Pietro Testa, Matteo Cagnoni *, Federica Cappelluti

Department of Electronics and Telecommunications, Politecnico di Torino, C.so Duca degli Abruzzi 24, Turin, 10129, Italy

ARTICLE INFO

Dataset link: https://doi.org/10.5281/zenodo.11210954

Keywords:
Multi-junction solar cells
Radiative cooling
Detailed-balance principle
Concentrating PV
BIPV and BICPV

ABSTRACT

Multi-junction solar cells are the best technology to achieve high-efficiency photovoltaics. Yet, their thermal management is crucial to ensure high performance and reliability, particularly in concentrating photovoltaic systems. Recent studies have proposed radiative cooling as an innovative, passive, cost-effective, and scalable technique to cool down solar cells. In this study, we analyze its impact on multi-junction solar cells under different illumination conditions by means of a detailed-balance model. First, we demonstrate that radiative cooling can provide greater efficiency gain in multi-junction devices than in single-junction ones despite the fact that the former heat up less than the latter. In fact, in multi-junction cells, the lower heating is more than compensated for by the stronger efficiency degradation with increasing temperature, due to their wider radiative recombination spectrum. Then, we explore two possible strategies to effectively use radiative cooling in low-concentration photovoltaic systems, such as building integrated concentrating photovoltaics. The first one is to combine the radiative cooler with a nonradiative cooling system, which then has relaxed performance requirements. The second one is to increase the radiative cooler area relative to that of the solar cell. Both approaches can provide significant performance benefits, whose magnitude depends on the selected design and application. For an optimal triple-junction cell under 10-sun concentration, we find that a radiative cooler having 5× the area of the solar cell reduces by 90% the nonradiative cooling power required to maintain the cell temperature at 60 °C and achieves +2% absolute efficiency gain over 1-sun operation.

1. Introduction

Multi-junction (MJ) solar cells are the best technology to date to surpass the Shockley–Queisser efficiency limit [1,2]. Several single-junction (SJ) sub-cells are stacked one above the other in order of increasing band gap, to obtain a trade-off between sub-gap photon transmission and thermalization of photogenerated charge carriers better than single-junction devices. In particular, thermalization leads to a high operating temperature that causes a degradation in performance. For instance, the relative efficiency of $In_{0.50}Ga_{0.50}P/In_{0.01}Ga_{0.99}As/Ge$ solar cells declines by about 0.33%/K [3], while the lifetime of a device is reduced by approximately two times for every 10 K of temperature increase [4]. These effects worsen in the case of concentrating photovoltaic (CPV) systems because of the higher heat loads.

Various passive and active cooling technologies have been developed over the years to improve the energy yield of solar cells by reducing their operating temperature [5]. They primarily rely on conductive and convective heat transfer mechanisms, such as heat sinks, forced airflow, and liquid cooling. However, the negative trade-off between complexity and performance-to-cost ratio of a commercial solar panel coupled with these cooling methods makes them unsuitable for widespread use beyond CPV systems [6,7].

Radiative heat transfer offers an attractive alternative or even complementary way to reduce the temperature of solar cells. It has been receiving increasing attention since 2014, when Raman et al. experimentally demonstrated that a body can radiatively cool down below ambient temperature under direct sunlight without any energy input [8]. This phenomenon is based on the coincidence of two physical facts that can be visualized with the help of Fig. 1: (1) Earth's atmosphere has a transparency window (AW) between 8 and 13 μm; (2) black body (BB) radiation has its peak within the atmospheric window at terrestrial temperatures. Because of this, a sky-facing body having high emissivity in the atmospheric window, the so-called radiative cooler (RC), is going to expel a large amount of heat into outer space through electromagnetic waves. Despite the equality between radiative cooler spectral absorbance and emissivity stated in Kirchhoff's law [9], this outgoing energy flux remains uncompensated in isothermal conditions, because little radiation is supplied by the atmosphere and the Sun

* Corresponding author.
E-mail address: matteo.cagnoni@polito.it (M. Cagnoni).

https://doi.org/10.1016/j.solmat.2024.112958
Received 7 March 2024; Received in revised form 18 May 2024; Accepted 22 May 2024
Available online 14 June 2024

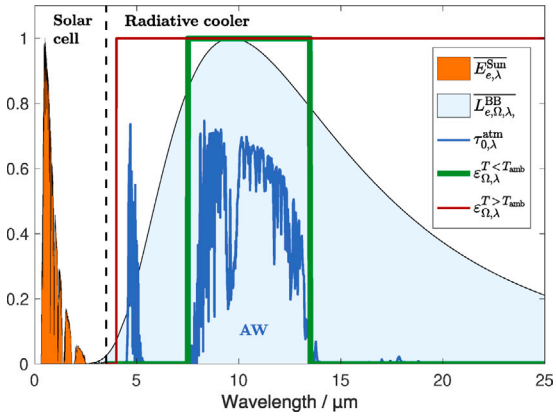

Fig. 1. Electromagnetic spectra involved in the radiative cooling mechanism. The red and green curve represents the radiative cooler ideal emissivity for cooling solar cells, $T > T_{amb}$, and for buildings applications, $T < T_{amb}$, respectively. The blue curve and area correspond to the zero-zenith atmospheric transmission spectrum and the black-body spectral radiance at 300 K. The orange curve is the standard solar spectrum AM1.5g.

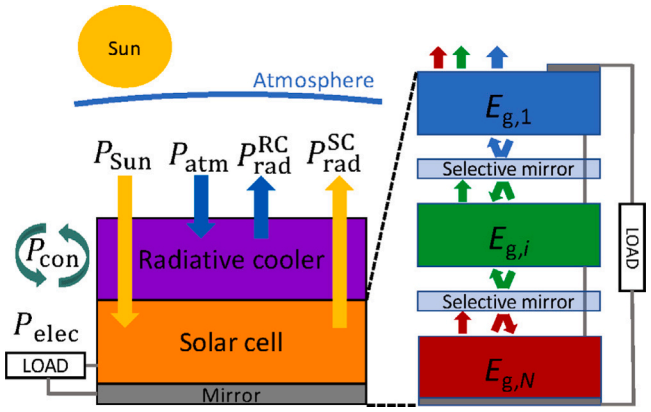

Fig. 2. Graphical representation of energy flows between radiative cooler, solar cell, Sun, and atmosphere. The schematic of the multi-junction solar cell is depicted on the right-hand side of the figure. The sub-cells are optically stacked and connected in series. Selective mirrors are placed between them to avoid electroluminescence coupling, and a perfect reflector is placed on the back of the device so that it emits only from the surface.

that can be re-absorbed by the radiative cooler at atmospheric window wavelengths. This energy imbalance leads the radiative cooler to spontaneously reduce its temperature until balance is restored.

As shown in Fig. 1, different optimal emissivity spectra can be identified to minimize the steady-state temperature, depending on the reachable temperature regime: (1) selective, with zero emissivity outside the atmospheric window, if sub-ambient temperature can be reached, such as in building applications; (2) broadband, if sub-ambient temperature cannot be reached, such as in photovoltaics. In the latter case, a radiative cooler with emissivity extended to the entire wavelength range between 4 and 30 μm and zero elsewhere maximizes cooling.

The possibility to develop a passive, lightweight, and integrable cooler for solar cells has attracted a growing interest from researchers. Several studies have focused on theoretically evaluating the impact of this technology on the cell performance and defining electromagnetic and thermal design requirements for an efficient radiative cooler [10–14]. Meanwhile, various materials with radiative cooling capability have been proposed and field tested, demonstrating their ability to reduce the solar cell temperature, although to different degrees depending on whether unencapsulated (bare) or encapsulated cells were considered [7,15–19]. In fact, encapsulated cells already exploit some amount of thermal radiation primarily because of the high emissivity of the cover glass [7,16–18]. Li et al. have estimated a temperature reduction of $8 \div 11$ °C in terrestrial environment, by applying an ideal radiative cooler to different types of encapsulated silicon cells [17], while smaller temperature reductions of $1 \div 2$ °C have been predicted by others [7,16,18]. The different results can be mostly attributed to the use of different data for the wavelength- and angular-dependence of the emissivity of the photovoltaic device. Overall, even though the actual gain enabled by optimizing the radiative cooling capability of current photovoltaic systems needs further scrutiny, there is a general consensus that a temperature reduction of a few degrees is worth pursuing, albeit challenging [16], and that higher gains can be expected in space and CPV applications [11,18,20]. In addition, radiative cooling emerges as an important aspect to consider in the development of novel designs and materials for photovoltaic applications where conventional encapsulation strategies are not suitable.

Most of previous works have studied single-junction solar cells and unconcentrated systems. In particular, we could find only one work dealing with the integration of MJ solar cells with a radiative cooler made of a micro-grating patterned glass [21], and few on the application of radiative cooling in single-junction cells for CPV [17,20,22].

On the other hand, recent improvements in manufacturing and the use of Earth-abundant materials are narrowing the gap in performance-to-cost ratio between MJ and commercial SJ solar cells [23,24]. As a result, the number of studies on the possible applications of this technology is growing. For example, low-concentrating photovoltaic systems for building integration (BICPV) have generated great interest because of design simplicity, little maintenance needs, and potentially higher performance-to-cost ratios [25–27].

Therefore, more studies on the application of radiative cooling to MJ solar cells in concentrating and non-concentrating systems are needed. Indeed, optimized radiative cooling could further increase their performance-to-cost ratio by enhancing their efficiency and extending their lifetime, hence fostering the widespread use of MJ solar cells and low-concentrating PV systems.

In this work, we explore the impact of ideal radiative cooling on MJ solar cells, with focus on low-concentrating photovoltaics, and provide a preliminary assessment of its performance limits. We propose a simple and general approach that allows us to encompass various implementations of the radiative cooler and different solar cells.

The system made of the solar cell and the radiative cooler depicted in Fig. 2 is described by a detailed-balance model, which includes the Shockley–Queisser (SQ) model for multi-junction solar cells with selective mirrors [28,29]. The mirrors limit the radiative coupling among sub-cells, leading to the highest limiting efficiency for any concentration factor [29]. The SQ model assumption of radiative recombination only and the use of selective mirrors lead to an underestimation of the cell heating, thus providing a worst-case scenario to assess the impact of radiative cooling in terms of temperature reduction and corresponding efficiency gain of the solar cell [30]. Furthermore, we focus on the series-connected two-terminal tandem cell, which is the most successfully implemented and up-scalable architecture to date.

In the following, we analyze the behavior of MJ solar cells integrating a radiative cooler for different numbers of junctions and operating conditions, considering unconcentrated and concentrated light with concentration up to 10-sun, which is a range of interest for BICPV applications [27]. In particular, we explore the possibility of combining the radiative cooler with other nonradiative cooling technologies to relax their design requirements, and investigate the impact of the ratio between the cooler and cell areas as a route to take advantage of radiative cooling under concentration and increase the cell efficiency [20,22].

2. Methods

We consider a structure consisting of a radiative cooler, a bare solar cell, and a perfect mirror. This system is depicted in Fig. 2, along with the power exchanges that occur when it is exposed to both solar and atmospheric radiation. Assuming that the temperature is uniform throughout the device, the net power density of the structure is given by:

$$P_{\text{net}} = P_{\text{rad}}^{\text{SC}} + P_{\text{elec}} - P_{\text{Sun}} + P_{\text{rad}}^{\text{RC}} - P_{\text{atm}} + P_{\text{con}} \tag{1}$$

$P_{\text{rad}}^{\text{SC}}$, P_{elec}, P_{Sun} correspond to the power density radiated, delivered to the load, and absorbed from the Sun by the solar cell, respectively. $P_{\text{rad}}^{\text{RC}}$ and P_{atm} are the power densities emitted and absorbed from the atmosphere by the radiative cooler. Finally, P_{con} defines the power density exchanged between the surrounding environment and the device through conduction and convection. By solving the equation $P_{\text{net}} = 0$, the steady-state temperature of the device is obtained. This allows us to evaluate the impact of the cooler on the solar cell by comparing the temperature with and without the radiative cooler, that is, with and without the terms $P_{\text{rad}}^{\text{RC}}$ and P_{atm}. The multi-junction architecture examined is the electrically constrained two-terminal tandem cell depicted on the right-hand side of Fig. 2. Its sub-cells are mechanically and optically stacked on top of each other so that the one facing the Sun has the widest band gap. We describe it through the detailed-balance model for multi-junction solar cells proposed in the works of De Vos [28], Henry [31], Martíand Araújo [29], and Futscher and Ehrler [32].

We make the following assumptions:

1. According to the SQ model, each sub-cell has unit absorbance for wavelengths shorter than $hc/E_{\text{g},i}$ and the band gaps are temperature-independent. In fact, the variation of the temperature coefficient due to the latter assumption is minimal in the typical temperature range of photovoltaics, as shown by Dupré et al. [33].
2. Selective mirrors are interposed between the sub-cells. These mirrors act as low-pass filters, reflecting light with energy higher than the overlying cell and letting through photons with lower energy. For instance, the reflectivity of the first mirror starting from the top of the solar cell is 1 for $E > E_{\text{g},1}$, 0 otherwise. Martíand Araújo have shown that this architecture slightly increases the radiative efficiency limit of MJ solar cells [29].
3. On the same grounds, an ideal mirror is placed at the back of the device.

The current-matching configuration determines that the current of the solar cell is set by the sub-cell producing the smallest current and that the voltage corresponds to the sum of the voltages of the sub-cells. Based on these considerations, the first three terms of Eq. (1) are calculated as follows:

$$P_{\text{rad}}^{\text{SC}} = \pi \int_0^{hc/E_{\text{g},1}} \mathrm{d}\lambda\, L_{e,\Omega,\lambda}^{\text{BB}}\left(\lambda, T, \text{V}_{1,\text{MPP}}\right) + \pi \sum_{i=2}^{N} \int_{hc/E_{\text{g},i-1}}^{hc/E_{\text{g},i}} \mathrm{d}\lambda\, L_{e,\Omega,\lambda}^{\text{BB}}\left(\lambda, T, \text{V}_{i,\text{MPP}}\right) \tag{2}$$

$$P_{\text{elec}} = J_{\text{MPP}} \cdot \sum_{i=1}^{N} V_{i,\text{MPP}} \tag{3}$$

$$P_{\text{Sun}} = \chi \int_0^{hc/E_{\text{g},N}} \mathrm{d}\lambda\, E_{e,\lambda}^{\text{Sun}}(\lambda) \tag{4}$$

$L_{e,\Omega,\lambda}^{\text{BB}}$ is the generalized Planck law derived by P. Wurfel [34], T is the temperature of the entire device, χ is the concentration factor, and $E_{e,\lambda}^{\text{Sun}}$ is the Sun spectral irradiance, for which we take the AM1.5g and AM1.5d spectra for the unconcentrated and concentrated case, respectively. Details on the model and the computation of the current and voltage terms can be found in section S1 of the Supplementary Material. Eq. (3) highlights that, by design, all the sub-cells are current-matched at maximum power point (MPP). Therefore, as the lowermost sub-cell energy gap changes, the set of band gaps of the MJ solar cell with the highest efficiency is found imposing that all the sub-cells operate at MPP with the same current.

The other actor in our device is the radiative cooler. We assume that it has the ideal emissivity for solar cell applications shown by the red curve in Fig. 1, that is, equal to 1 for $\lambda \geq 4$ μm, and 0 elsewhere. Furthermore, it is perfectly transparent in the UV–visible range, so as not to interfere with the absorption of sunlight by the solar cell. The radiative cooler can be positioned either above or below the solar cell because the two elements are electromagnetically independent and only thermally coupled. The atmospheric radiated power absorbed by the radiative cooler and the power it emits are given by:

$$P_{\text{atm}} = f_A \times \int \mathrm{d}\Omega \cos\theta \int_0^{+\infty} \mathrm{d}\lambda\, \varepsilon_{\Omega,\lambda}^{\text{atm}}(\lambda,\theta)\, \varepsilon_{\Omega,\lambda}^{\text{RC}}(\lambda,\theta)\, L_{e,\Omega,\lambda}^{\text{BB}}\left(\lambda, T_{\text{amb}}, 0\right) \tag{5}$$

$$P_{\text{rad}}^{\text{RC}} = f_A \int \mathrm{d}\Omega \cos\theta \int_0^{+\infty} \mathrm{d}\lambda\, \varepsilon_{\Omega,\lambda}^{\text{RC}}(\lambda,\theta)\, L_{e,\Omega,\lambda}^{\text{BB}}(\lambda, T, 0) \tag{6}$$

$\varepsilon_{\Omega,\lambda}^{\text{RC}}$ and $\varepsilon_{\Omega,\lambda}^{\text{atm}}$ are the spectral directional emissivities of the radiative cooler and the atmosphere. We obtain the latter according to the formula $\varepsilon_{\Omega,\lambda}^{\text{atm}} = 1 - \tau_{0,\lambda}^{\text{atm}\,1/\cos\theta}$, where $\tau_{0,\lambda}^{\text{atm}}$ is the zero-zenith spectral transmittance calculated from the summer spectrum included in RadCool [35] from MODTRAN [36]. T_{amb} is ambient temperature and is equal to 293.15 K. θ is the zenith angle associated with the z-axis normal to the surface of the solar cell. For our computation, we assume that the radiative cooler emits isotropically and only in the upper hemisphere due to the presence of the mirror at the back. f_A is the ratio between the radiative cooler and solar cell areas, that is:

$$f_A = A_{\text{RC}}/A_{\text{SC}} \tag{7}$$

This parameter helps us to investigate how the radiative cooler performance varies as its area increases with respect to that of the solar cell. We use it in the case of concentrated light, envisioning the radiative cooler placed underneath the solar cell, as in some configurations reported in literature [14,20,22]. In this case, the solar cell area is smaller than that of the module, thus the maximum radiative cooler area is limited only by the size of the concentrator.

Finally, nonradiative heat transfer is modeled as:

$$P_{\text{con}} = f_A\, h_{\text{c}}(T - T_{\text{amb}}) \tag{8}$$

h_{c} is an effective nonradiative heat transfer coefficient accounting for possible conductive and convective mechanisms between the system and the surrounding environment. It is usually obtained experimentally and depends greatly on the operating conditions, such as wind speed, mounting configuration, and the shape and material of the device [20]. By varying this coefficient, we could evaluate the impact of the radiative cooler used in conjunction with other cooling technologies, such as a backside finned heatsink, or under different wind conditions. To this end, we defined h_{c} as $h_{\text{c0}} + \Delta h_{\text{c}}$, where h_{c0} is set to the well-established value of 10.6 W m^{-2} K^{-1} for a rectangular flat plate structure in case of average wind [12], and Δh_{c} corresponds to the variation from this reference condition. The nonradiative power density is scaled proportionally to the area of the largest available surface, that is, the radiative cooler one, according to our assumptions.

It is worth mentioning that the model provides a reasonable estimate of the temperature as long as the isothermal assumption between and within the radiative cooler and the cell is valid. Factors such as limited heat diffusion length and thermal contact between the solar cell and the radiative cooler can become critical for some actual structures. As the thermal conductivity and geometrical factors come into play, accurate thermal analysis may require a thermal simulation of the device based on numerical methods, such as the finite element method, which is beyond the scope of the present work.

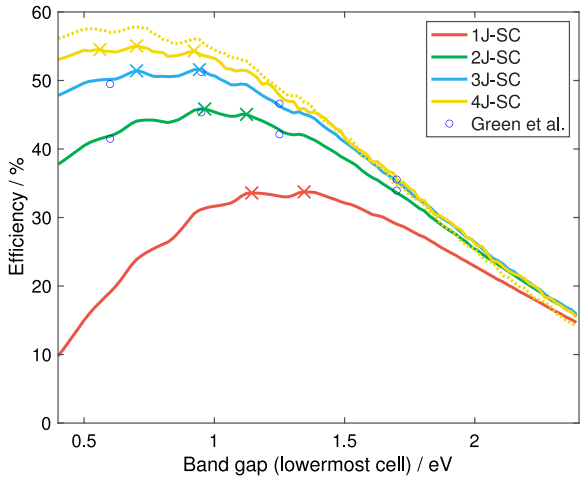

Fig. 3. Efficiency of series-connected stacked tandem cells with different numbers of junctions under unconcentrated (solid lines) and 10-sun concentrated light (dashed line, 4J-SC) as a function of the band gap of the lowermost cell. Calculations assume an operating temperature of 300 K and AM1.5g (unconcentrated case) and AM1.5d (10-sun) spectra. Crosses highlight calculated efficiency peaks.
Source: Circles are calculated data from [37].

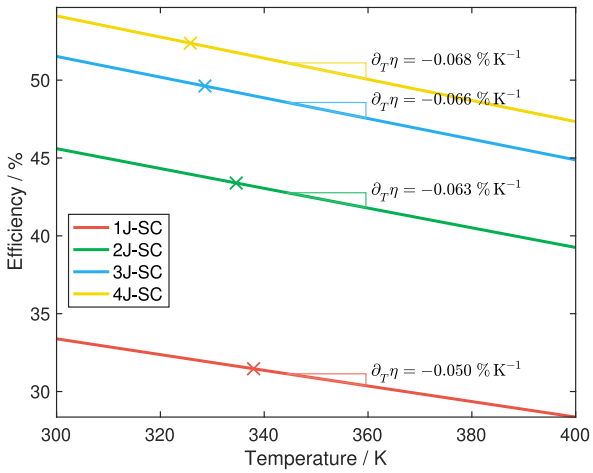

Fig. 4. Temperature dependence of the efficiency of solar cells with different numbers of junctions under unconcentrated light. The solar cells considered have $E_g^{\text{bottom}} = 1.12\,\text{eV}$ for the one-junction case and $E_g^{\text{bottom}} = 0.93\,\text{eV}$ for the others (see Table S1 in Supplementary Material). The absolute temperature coefficients are reported together with the operating temperature of solar cells (colored crosses). The curves are calculated using the AM1.5g spectrum.

3. Results and discussion

To support the following discussion, we report in Fig. 3 the calculated efficiency of multi-junction solar cells with different numbers of junctions as a function of the energy gap of the lowermost cell (E_g^{bottom}). The results agree well with previous studies, validating the model [32,37,38] (blue circles in Fig. 3). As the number of junctions increases, the thermalization losses are reduced and the MJ solar cell can exploit a larger portion of the solar spectrum, with a red-shift of the optimal lowermost band gap, whose corresponding peak in the efficiency vs lowermost gap plot becomes higher and broader. These characteristics are emphasized by the colored crosses in Fig. 3, which mark the local efficiency maxima of the unconcentrated case. Solar cells under low-concentrated light exhibit the same qualitative behavior. For instance, the dashed yellow line in Fig. 3 represents the efficiency of four-junction solar cells designed for a 10-sun application.

3.1. Effect of temperature on MJ-SCs

The detailed-balance model of multi-junction solar cells allows us to investigate their temperature sensitivity and to develop a basic understanding of the physics underlying it. To this end, we consider solar cells with two, three, and four junctions that absorb almost the same part of the solar spectrum and compare their behavior in temperature with respect to a single-junction solar cell made of c-Si. In particular, we choose the optimal configuration of energy gaps with E_g^{bottom} set at 0.93 eV, a value that approximately corresponds to the local efficiency maximum closest to the silicon band gap, regardless of the number of junctions (see Table S1 in Supplementary Material). Fig. 4 depicts the efficiency calculated through the Shockley–Queisser model for multi-junction solar cells (see Supplementary Material S1). The efficiency decreases with temperature because of increased radiative recombination, with linear behavior. The absolute temperature coefficient $\partial_T\eta$, which corresponds to the slope of the curve, reveals that the efficiency reduction is more pronounced for a larger number of junctions. Such behavior stems from the increased rate of radiative recombination at higher temperatures and with more junctions, as described by Eq. (2). Indeed, the power radiated by the solar cell grows with temperature according to the generalized Planck law, causing voltage and fill factor losses [39]. This mechanism is amplified in the multi-junction architecture, because the emission losses of each sub-cell add up, increasing the overall power radiated by the stack, as shown by Eq. (2). Moreover, this equation implies that the temperature coefficient increases as the energy gap of the bottom cell decreases. In other words, solar cells with a broader emissivity spectrum emit more photons at a given temperature, which makes them more sensitive to temperature changes.

As the multi-junction architecture reduces self-heating, we would expect the steady-state temperature of these devices to decrease with increasing number of junctions. To demonstrate this, we solve $P_{\text{net}} = 0$ without the terms related to the radiative cooler, implying that natural convection (P_{con}) is the only cooling mechanism. The obtained (T, η) working points for different numbers of junctions are represented as crosses in Fig. 4. As anticipated, the steady-state temperature shifts towards lower values by increasing the number of junctions because, for the chosen bang gap configurations, all solar cells absorb nearly the same portion of the solar spectrum regardless of the number of junctions, but those with more junctions convert a larger fraction of the harvested energy into electrical energy.

Because of the difference between the AM1.5g and AM1.5d spectra and of light concentration, the configuration of energy gaps for maximum efficiency changes in CPV. In particular, the top cells have smaller band gaps. However, the absolute temperature coefficient as a function of the number of junctions follows the same trend as in the unconcentrated case. Fig. 5 illustrates this aspect and shows the significant dependence of the coefficient on the illumination conditions. This figure is obtained using the sets of band gaps calculated for a concentration of 10-sun and selected according to the same criteria used previously (see Table S1 in Supplementary Material). Interestingly, the greater the concentration factor, the less sensitive the solar cell is to temperature variations. For a solar cell under concentrated light, the recombination rate at maximum power point significantly increases due to the larger density of photogenerated carriers. As consequence, the relative weight of temperature-induced variations of the radiative recombination rate significantly diminishes compared to the unconcentrated case. To put it simply, the higher open-circuit voltage under concentration reduces temperature-induced efficiency losses. Moreover, since the increase in open-circuit voltage occurs in every sub-cell of the stack, the reduction in $\partial_T\eta$ becomes more significant with increasing

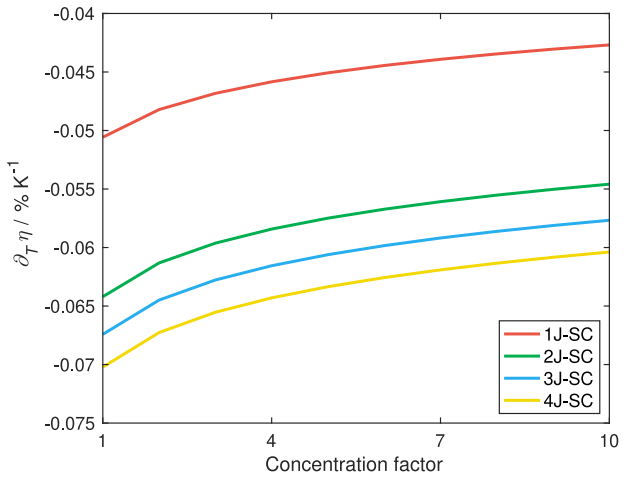

Fig. 5. Absolute temperature coefficient of efficiency of solar cells with different numbers of junctions as a function of the concentration factor. The solar cells considered have $E_g^{bottom} = 1.12\,eV$ for the one-junction case and $E_g^{bottom} = 0.93\,eV$ for the others (see Table S1 in Supplementary Material). The curves are calculated using the AM1.5d spectrum.

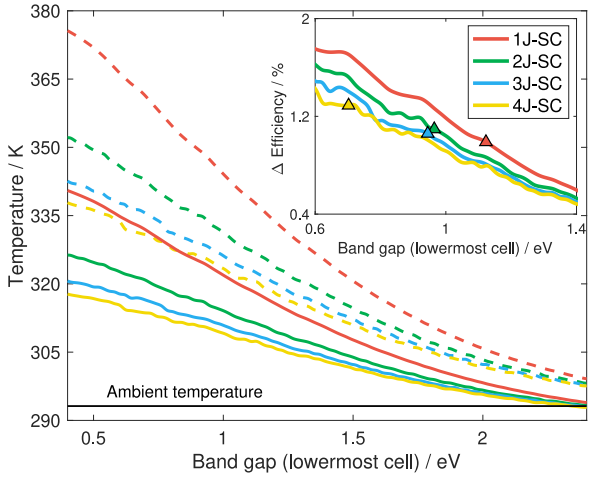

Fig. 6. Operating temperature of solar cells without (dashed lines) and with (solid lines) radiative cooler under unconcentrated light for different numbers of junctions and as a function of the energy gap of the lowermost cell. The inset shows the increase in solar cell efficiency achieved thanks to the radiative cooler, that is, ΔEfficiency = $\text{Efficiency}_{\text{SC w/ RC}} - \text{Efficiency}_{\text{SC}}$. In particular, the triangles indicate the improvements obtained in the case of the most efficient MJ and c-Si solar cells (see Fig. 3). The curves are calculated by solving $P_{net} = 0$ with $h_c = 10.6\,Wm^{-2}K^{-1}$, $T_{amb} = 293.15\,K$, $f_A = 1$, and under AM1.5g illumination.

number of junctions for a specific concentration factor (see further details in Supplementary Material S2).

Based on these considerations, the absolute temperature coefficients of MJ solar cells have lower values in the concentrated case for a given number of junctions, as shown by comparing their values in Figs. 4 and 5. These results are in agreement with both theoretical and experimental findings reported in the literature [3,40]. Further details on the effect of temperature on the photovoltaic figures of merit can be found in section S3 of the Supplementary Material.

3.2. Impact of a radiative cooler on MJ-SCs under unconcentrated light

Fig. 6 compares the steady-state temperature of 1J to 4J solar cells with and without the radiative cooler, under unconcentrated light, calculated as a function of the band gap of the lowermost cell. Equal cell/cooler areas and standard outdoor conditions, that is, $f_A = 1$ and $\Delta h_c = 0$, are assumed. The temperature reduction provided by the radiative cooler is more significant at small band gaps and for fewer junctions because of the stronger heating of the solar cell and the associated increase in thermal radiation by the RC. High-efficiency multi-junction solar cells are located at these band gaps, as shown in Fig. 3, making the radiative cooler suitable for their thermal management. The inset of Fig. 6 shows the efficiency improvements as a function of the energy gap of the bottom cell, resulting from the RC-driven temperature reduction. The efficiency gain at fixed bottom gap decreases as the number of junctions increases, despite the more negative temperature coefficients. However, the colored triangles in the inset, which correspond to the optimal bottom gap values for each number of junctions, show that the most efficient multi-junction solar cells reach comparable or even higher efficiency gains than silicon SJ ones. For instance, the radiative cooler passively reduces the temperature of the 4J-SC with maximum efficiency (yellow triangle in Fig. 6) by 17 K, leading to an increase of about 1.3% in absolute efficiency, from 52.7% to 54%, and an extension of the lifetime by more than three times, according to the Arrhenius law. On the other hand, the temperature reduction of c-Si SJ solar cells (red triangle) is about 19 K, which corresponds to an increase of about 1% in absolute efficiency, and a slightly higher lifetime extension. These results are in line with previous theoretical works [10,21] on bare solar cells and confirm that optimizing radiative cooling is important for the thermal management of both single-junction and multi-junction solar cells. Outdoor field tests reported by Heo et al. [21] on 3J solar cells demonstrated a temperature reduction of 4.7 and 6.1 K for a cell integrating a photonic radiative cooler, with respect to a conventional glass-mounted cell and an unencapsulated one, respectively. This corresponds to about one-third of the reduction calculated by the detailed balance model. Although this can be partly attributed to non-idealities of the experiment, it might also indicate that the two reference cells were already somewhat cooled by thermal emission. In fact, recent studies have pointed out that the thermal emissivity of unencapsulated silicon cells can be higher than what usually assumed based on the optical properties of silicon wafers, due to the influence of highly doped layers and surface texturing [41,42]. In this regard, further studies should be conducted to elucidate the thermal emissivity of both encapsulated and unencapsulated solar cells, in order to better quantify the potential gain offered by optimized radiative cooling in a given photovoltaic technology.

3.3. Impact of a radiative cooler on MJ-SCs under low-concentrated light

It is worth investigating the application of radiative cooling also to low-concentrating photovoltaic systems, as they exhibit higher heat loads and hence require careful thermal management. To this end, we start by considering the same structure as before, that is, a planar cell/cooler stack with $f_A = 1$ ($A_{RC} = A_{SC}$), but subject to AM1.5d illumination; we consider concentration factors between 1 and 10 sun. For the sake of brevity, we only discuss the three-junction case in the main text and refer the reader to the Supplementary Material S4 for the other cases.

Fig. 7 shows the three-junction solar cell operating temperature calculated as a function of its bottom band gap when exposed to different concentration levels, with the other band gaps optimized at concentration level $\chi = 10$. As expected, the system temperature dramatically increases under concentration, reaching extremely high values for $\chi > 2$. As consequence, the cooler radiates a large amount of energy and induces a significant temperature reduction, which becomes more prominent for fewer junctions (see Supplementary Material S4). For instance, the temperature reduction in the most efficient 3J-SC is about 35 K and 122 K for $\chi = 2$ and $\chi = 5$, respectively. Despite this enormous heat removal, the operating temperature of the cell remains

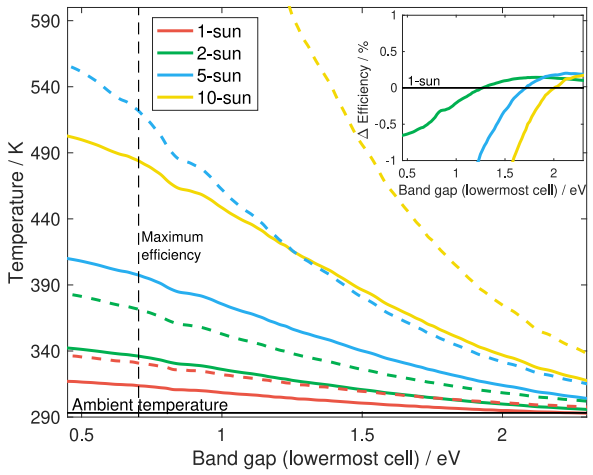

Fig. 7. Operating temperature of three-junction solar cells without (dashed lines) and with (solid lines) radiative cooler under direct sunlight for different concentration factors and as a function of the energy gap of the lowermost cell. For the case study with radiative cooler, the inset shows the difference between the efficiency of the solar cell operating under various concentration factors and the one at 1-sun, that is, ΔEfficiency = Efficiency$_{\chi-\text{sun}}$ − Efficiency$_{1\text{-sun}}$ for $\chi > 1$. T crossing of the zero (black curve) indicates the point at which the solar cell under concentrated light has a higher efficiency than at 1-sun. The curves are calculated by solving $P_{\text{net}} = 0$ with $h_c = 10.6\,\text{Wm}^{-2}\text{K}^{-1}$, $T_{\text{amb}} = 293.15\,\text{K}$, $f_A = 1$, under AM1.5d illumination.

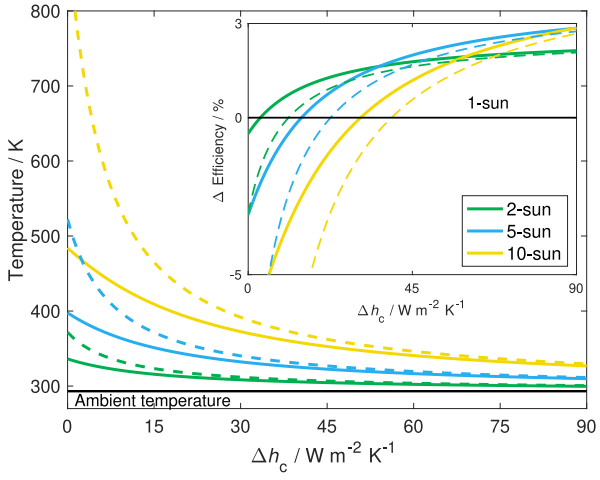

Fig. 8. Operating temperature of the highest-efficiency three-junction solar cell without (dashed lines) and with (solid lines) radiative cooler for different concentration factors as a function of the increment of the nonradiative heat transfer coefficient, Δh_c. For the case study with radiative cooler, the inset shows the difference between the efficiency of the solar cell operating under various concentration factors and the one at 1-sun and for $\Delta h_c = 0$, that is, ΔEfficiency = Efficiency$_{\chi-\text{sun}}$ − Efficiency$_{1\text{-sun}}$ for $\chi > 1$. The curves are calculated by solving $P_{\text{net}} = 0$ with $h_{c0} = 10.6\,\text{Wm}^{-2}\text{K}^{-1}$, $T_{\text{amb}} = 293.15\,\text{K}$, $f_A = 1$, under AM1.5d illumination.

too high, that is, above the acceptable limit of about 110 °C [20]. As consequence, the efficiency is lower than the one under unconcentrated light. This is highlighted in the inset of Fig. 7, where we show the difference between the efficiency, at steady-state temperature, of the three-junction solar cells coupled with the radiative cooler under various concentration levels, and the efficiency of the same solar cell at 1-sun. Under concentrated light, the device becomes slightly more efficient than in the unconcentrated case only for high band gaps, which however correspond to low-efficiency devices.

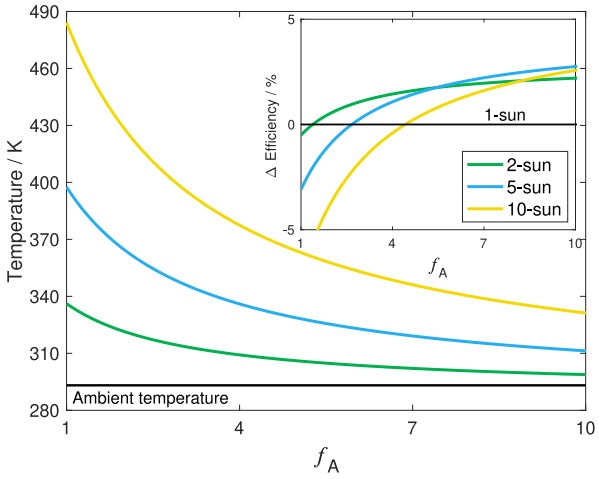

Fig. 9. Operating temperature of the highest-efficiency three-junction solar cell coupled with radiative cooler for different concentration factors as a function of the ratio between RC and SC area (see Eq. (7)). The inset shows the difference in efficiency between cells operating under various concentration factors and the one at 1-sun and for $f_A = 1$, that is, ΔEfficiency = Efficiency$_{\chi-\text{sun}}$ − Efficiency$_{1\text{-sun}}$ for $\chi > 1$. The curves are calculated by solving $P_{\text{net}} = 0$ with $h_c = 10.6\,\text{Wm}^{-2}\text{K}^{-1}$, $T_{\text{amb}} = 293.15\,\text{K}$, under AM1.5d illumination.

We consider two possible approaches to further reduce the operating temperature: (1) combining the radiative cooler with a nonradiative cooling system, such as a conductive finned aluminum plate [20,43]; (2) increasing the area of the radiative cooler beyond that of the solar cell, as experimentally done in [20,22] for a single-gap solar cell. To evaluate the effectiveness of these strategies, we take the three-junction solar cell that is most efficient under 1-sun (top-to-bottom gaps: 1.75/1.18/0.70 eV) as benchmark.

Let us start with the first approach. Fig. 8 depicts the operating temperature decrease of the three-junction solar cell as the strength of conductive/convective mechanisms increases, for different concentration factors. Δh_c is varied from 0 to 90 W m^{-2}K^{-1} because these are typical values for common cooling mechanisms [44]. The zero on the horizontal axis corresponds to the normal environmental conditions considered so far, that is, $h_c = 10.6$ W m^{-2} K^{-1}. The contribution of the radiative cooler to the temperature reduction remains significant despite the nonradiative terms taking over part of the task, especially for high-concentration factors. For example, the additional temperature reduction provided by an ideal radiative cooler to the 3J-SC under 5-sun for $\Delta h_c = 10$ W m^{-2} K^{-1}, which has been measured by Wang et al. and corresponds to a finned heat sink and a wind speed of 6 m s^{-1}, is about 30 K. This corresponds to a remarkable 2% increase in absolute efficiency. The smoothing of the temperature curves and the progressive reduction of the radiative cooler impact stem from the predominance of nonradiative heat transfer mechanisms for high Δh_c values (see Eq. (8)), for which the solar cell temperature approaches ambient one. In addition to these results, the inset of Fig. 8 allows to estimate the nonradiative heat transfer coefficient required to overcome the efficiency of the unconcentrated case, whose value grows with concentration factor. It is noteworthy that the temperature reduction induced by the radiative cooler considerably reduces the h_c needed, relaxing the requirements for the cooling system. For example, a 3J solar cell without radiative cooler under 10-sun needs $h_c > 50$ W m^{-2} K^{-1} to surpass its efficiency under 1-sun. This requirement is reduced to $h_c > 40$ W m^{-2} K^{-1} if the solar cell is coupled to a radiative cooler. Interestingly, the value of h_c needed to reach the same efficiency as the 1-sun case does not vary significantly if one considers the most efficient solar cell for each number of junctions (see Supplementary Material S4).

The second approach is especially interesting for CPV, as shown in [20,22], because the solar cell is smaller in size than the concentrator system. The greater surface area of the radiative cooler favors radiative and nonradiative heat transfer mechanisms. This results in a reduction of the operating temperature of the solar cell dependent on the ratio between the cooler and cell areas (f_A), as shown in Fig. 9. Here, we use as upper limit for f_A the concentration factor, considering it as representative of the concentrating system size. However, in practical systems the concentrator size is slightly larger than the concentration factor to compensate for optical and geometrical loss of the concentrating system.

The inset of Fig. 9 illustrates that the temperature drop induced by increasing the radiative cooler area enables the solar cell under concentration to significantly exceed the efficiency of the unconcentrated case. For example, under 10-sun, the use of a radiative cooler with area comparable to that one of the concentrating system allows for an operating temperature of about 40 °C (i.e. 150 °C of temperature reduction with respect to the case $f_A = 1$), corresponding to nearly 4% absolute efficiency gain with respect to operation under 1-sun.

As in the previous approach, the temperature reduction provided by the radiative cooler is almost independent of the number of junctions when considering solar cells with optimal band gaps. What varies from one cell to another is the increase in efficiency, which is strongly influenced by the temperature coefficients (see Supplementary Material S4). The high temperature reduction enabled by the larger radiative cooler surface suggests that this approach could be effective at limiting the solar cell operating temperature at acceptable values even for moderate concentration levels, provided that the thermal diffusion length of the radiative cooler is greater than its size.

4. Conclusions

We have presented an assessment of the theoretical performance of radiatively cooled multi-junction solar cells operating under unconcentrated and low-concentrated light. The analysis of the solar cell thermal behavior, studied using a detailed-balance approach, reveals that their temperature coefficient of efficiency significantly depends on the solar cell architecture, materials, and illumination conditions. In particular, as the number of junctions increases and the optimal energy gap of the bottom cell decreases, the absolute temperature coefficient of the efficiency becomes more negative because of the cumulative effect of emission loss from each sub-cell and the wider emissivity of the device. For this reason, although multi-junction solar cells heat up less than their single-junction counterparts, the impact of radiative cooling on their performance is comparable to, if not greater than, the one found in single-junction devices, even under unconcentrated light conditions.

In low-concentrating applications (χ ranges from 1-sun to 10-sun), we have shown that the radiative cooler does not provide enough cooling power to lower the temperature to acceptable values when it has the same area as the solar cell and is used as the only cooling mechanism. However, it can offer an attractive approach for thermal management when combined with other nonradiative cooling mechanisms, significantly reducing their design requirements. Moreover, large temperature reductions can be achieved by increasing the surface area of the cooler relative to that of the solar cell. Along with its high integrability, these results suggest that radiative cooling is an important element in the thermal management of CPV systems from low to moderate concentration levels.

Finally, the integration of radiative coolers in PV systems not only improves efficiency, but also extends their lifetime, leading to a higher overall energy production that can contribute to fostering their large-scale implementation.

The presented model assumes that the solar cell itself has negligible thermal emissivity, but has perfect thermal coupling with the radiative cooler. Therefore, the calculated operating temperature and efficiency of the integrated system consisting of radiative cooler and solar cell are also representative of a solar cell with ideal thermal emissivity. On the other hand, the specific gain allowed by the integration of a radiative cooler in the photovoltaic system architecture needs to be further refined by taking into account realistic thermal emissivities of the selected system components.

CRediT authorship contribution statement

Pietro Testa: Writing – review & editing, Writing – original draft, Visualization, Validation, Software, Methodology, Investigation, Formal analysis, Data curation, Conceptualization. **Matteo Cagnoni:** Writing – review & editing, Validation, Supervision, Project administration, Methodology, Conceptualization. **Federica Cappelluti:** Writing – review & editing, Validation, Supervision, Project administration, Methodology, Funding acquisition, Conceptualization.

Declaration of competing interest

The authors declare that they have no known competing financial interests or personal relationships that could have appeared to influence the work reported in this paper.

Data availability

The codes and data that support the findings of this study are available in Zenodo at https://doi.org/10.5281/zenodo.11210954.

Acknowledgments

This project has received funding from the European Union's Horizon 2020 Research and Innovation Program under grant agreement No. 964450.

Appendix A. Supplementary data

Supplementary material related to this article can be found online at https://doi.org/10.1016/j.solmat.2024.112958.

References

[1] Best research-cell effficiency chart. URL: https://www.nrel.gov/pv/cell-efficiency.html.
[2] W. Shockley, H.J. Queisser, Detailed balance limit of efficiency of *p-n* junction solar cells, J. Appl. Phys. 32 (3) (1961) 510–519, http://dx.doi.org/10.1063/1.1736034.
[3] G. Siefer, A.W. Bett, Analysis of temperature coefficients for III–V multi-junction concentrator cells, Prog. Photovolt., Res. Appl. 22 (5) (2014) 515–524, http://dx.doi.org/10.1002/pip.2285, _eprint: https://onlinelibrary.wiley.com/doi/pdf/10.1002/pip.2285.
[4] O. Dupré, R. Vaillon, M.A. Green, Thermal Behavior of Photovoltaic Devices, Springer International Publishing, Cham, 2017, http://dx.doi.org/10.1007/978-3-319-49457-9, URL: http://link.springer.com/10.1007/978-3-319-49457-9.
[5] P. Dwivedi, K. Sudhakar, A. Soni, E. Solomin, I. Kirpichnikova, Advanced cooling techniques of P.V. modules: A state of art, Case Stud. Therm. Eng. 21 (2020) 100674, http://dx.doi.org/10.1016/j.csite.2020.100674.
[6] A. Royne, C.J. Dey, D.R. Mills, Cooling of photovoltaic cells under concentrated illumination: a critical review, Sol. Energy Mater. Sol. Cells 86 (4) (2005) 451–483, http://dx.doi.org/10.1016/j.solmat.2004.09.003.
[7] D. Sato, N. Yamada, Review of photovoltaic module cooling methods and performance evaluation of the radiative cooling method, Renew. Sustain. Energy Rev. 104 (2019) 151–166, http://dx.doi.org/10.1016/j.rser.2018.12.051.
[8] A.P. Raman, M.A. Anoma, L. Zhu, E. Rephaeli, S. Fan, Passive radiative cooling below ambient air temperature under direct sunlight, Nature 515 (7528) (2014) 540–544, http://dx.doi.org/10.1038/nature13883.
[9] C. Balaji, Essentials of Radiation Heat Transfer, Springer International Publishing, Cham, 2021, http://dx.doi.org/10.1007/978-3-030-62617-4, URL: http://link.springer.com/10.1007/978-3-030-62617-4.
[10] L. Zhu, A. Raman, K.X. Wang, M.A. Anoma, S. Fan, Radiative cooling of solar cells, Optica 1 (1) (2014) 32, http://dx.doi.org/10.1364/OPTICA.1.000032.
[11] T.S. Safi, J.N. Munday, Improving photovoltaic performance through radiative cooling in both terrestrial and extraterrestrial environments, Opt. Express 23 (19) (2015) A1120, http://dx.doi.org/10.1364/OE.23.0A1120.

[12] G. Perrakis, A.C. Tasolamprou, G. Kenanakis, E.N. Economou, S. Tzortzakis, M. Kafesaki, Passive radiative cooling and other photonic approaches for the temperature control of photovoltaics: A comparative study for crystalline silicon-based architectures, Opt. Express 28 (13) (2020) 18548, http://dx.doi.org/10.1364/OE.388208.

[13] J. Dumoulin, E. Drouard, M. Amara, Radiative sky cooling of solar cells: fundamental modelling and cooling potential of single-junction devices, Sustain. Energy Fuels 5 (7) (2021) 2085–2096, http://dx.doi.org/10.1039/D0SE01536A, Publisher: The Royal Society of Chemistry.

[14] M. Cagnoni, A. Tibaldi, J.S. Dolado, F. Cappelluti, Cementitious materials as promising radiative coolers for solar cells, iScience (2022) 105320, http://dx.doi.org/10.1016/j.isci.2022.105320.

[15] L. Zhu, A.P. Raman, S. Fan, Radiative cooling of solar absorbers using a visibly transparent photonic crystal thermal blackbody, Proc. Natl. Acad. Sci. 112 (40) (2015) 12282–12287, http://dx.doi.org/10.1073/pnas.1509453112, Publisher: Proceedings of the National Academy of Sciences.

[16] A. Gentle, G. Smith, Is enhanced radiative cooling of solar cell modules worth pursuing? Sol. Energy Mater. Sol. Cells 150 (2016) 39–42.

[17] W. Li, Y. Shi, K. Chen, L. Zhu, S. Fan, A comprehensive photonic approach for solar cell cooling, ACS Photon. 4 (4) (2017) 774–782, http://dx.doi.org/10.1021/acsphotonics.7b00089.

[18] B. Zhao, M. Hu, X. Ao, G. Pei, Performance analysis of enhanced radiative cooling of solar cells based on a commercial silicon photovoltaic module, Sol. Energy 176 (2018) 248–255.

[19] S. Lin, L. Ai, J. Zhang, T. Bu, H. Li, F. Huang, J. Zhang, Y. Lu, W. Song, Silver ants-inspired flexible photonic architectures with improved transparency and heat radiation for photovoltaic devices, Sol. Energy Mater. Sol. Cells 203 (2019) 110135, http://dx.doi.org/10.1016/j.solmat.2019.110135.

[20] Z. Wang, D. Kortge, J. Zhu, Z. Zhou, H. Torsina, C. Lee, P. Bermel, Lightweight, passive radiative cooling to enhance concentrating photovoltaics, Joule 4 (12) (2020) 2702–2717, http://dx.doi.org/10.1016/j.joule.2020.10.004.

[21] S.-Y. Heo, D.H. Kim, Y.M. Song, G.J. Lee, Determining the effectiveness of radiative cooler-integrated solar cells, Adv. Energy Mater. 12 (10) (2022) 2103258, http://dx.doi.org/10.1002/aenm.202103258, _eprint: https://onlinelibrary.wiley.com/doi/pdf/10.1002/aenm.202103258.

[22] Z. Zhou, Z. Wang, P. Bermel, Radiative cooling for low-bandgap photovoltaics under concentrated sunlight, Opt. Express 27 (8) (2019) A404–A418, http://dx.doi.org/10.1364/OE.27.00A404, Publisher: Optica Publishing Group.

[23] M. Yamaguchi, F. Dimroth, J.F. Geisz, N.J. Ekins-Daukes, Multi-junction solar cells paving the way for super high-efficiency, J. Appl. Phys. 129 (24) (2021) 240901, http://dx.doi.org/10.1063/5.0048653.

[24] A. Baiju, M. Yarema, Status and challenges of multi-junction solar cell technology, Front. Energy Res. 10 (2022).

[25] D. Chemisana, Building integrated concentrating photovoltaics: A review, Renew. Sustain. Energy Rev. 15 (1) (2011) 603–611, http://dx.doi.org/10.1016/j.rser.2010.07.017.

[26] G. Li, Q. Xuan, M. Akram, Y. Golizadeh Akhlaghi, H. Liu, S. Shittu, Building integrated solar concentrating systems: A review, Appl. Energy 260 (2020) 114288, http://dx.doi.org/10.1016/j.apenergy.2019.114288.

[27] R.V. Parupudi, H. Singh, M. Kolokotroni, Low concentrating photovoltaics (LCPV) for buildings and their performance analyses, Appl. Energy 279 (2020) 115839, http://dx.doi.org/10.1016/j.apenergy.2020.115839.

[28] A.D. Vos, Detailed balance limit of the efficiency of tandem solar cells, J. Phys. D: Appl. Phys. 13 (1980) 839.

[29] A. Martí, G.L. Araújo, Limiting efficiencies for photovoltaic energy conversion in multigap systems, Sol. Energy Mater. Sol. Cells 43 (2) (1996) 203–222, http://dx.doi.org/10.1016/0927-0248(96)00015-3.

[30] M. Cagnoni, P. Testa, J.S. Dolado, F. Cappelluti, Extended detailed balance modeling toward solar cells with cement-based radiative coolers, Prog. Photovolt., Res. Appl. n/a (n/a) (2023) http://dx.doi.org/10.1002/pip.3758, _eprint: https://onlinelibrary.wiley.com/doi/pdf/10.1002/pip.3758.

[31] C.H. Henry, Limiting efficiencies of ideal single and multiple energy gap terrestrial solar cells, J. Appl. Phys. 51 (8) (1980) 4494–4500, http://dx.doi.org/10.1063/1.328272, Publisher: American Institute of Physics.

[32] M.H. Futscher, B. Ehrler, Efficiency limit of perovskite/Si tandem solar cells, ACS Energy Lett. 1 (4) (2016) 863–868, http://dx.doi.org/10.1021/acsenergylett.6b00405, Publisher: American Chemical Society.

[33] O. Dupré, B. Niesen, S. De Wolf, C. Ballif, Field performance versus standard test condition efficiency of tandem solar cells and the singular case of perovskites/silicon devices, J. Phys. Chem. Lett. 9 (2) (2018) 446–458, http://dx.doi.org/10.1021/acs.jpclett.7b02277.

[34] P. Wurfel, The chemical potential of radiation, J. Phys. C 15 (18) (1982) 3967, http://dx.doi.org/10.1088/0022-3719/15/18/012.

[35] Y.-w. Lin, E. Schlenker, Z. Zhou, P. Bermel, RadCool: a web-enabled simulation tool for radiative cooling, in: The Summer Undergraduate Research Fellowship (SURF) Symposium, 2017.

[36] A. Berk, G. Anderson, K. Acharya, L. Bernstein, L. Muratov, J. Lee, M. Fox, S. Adler-Golden, J. Jr., M. Hoke, R. Lockwood, J. Gardner, MODTRAN5: 2006 update, Proc. SPIE - Int. Soc. Opt. Eng. 6233 (2006) http://dx.doi.org/10.1117/12.665077.

[37] M.A. Green, S.P. Bremner, Energy conversion approaches and materials for high-efficiency photovoltaics, Nature Mater. 16 (1) (2017) 23–34, http://dx.doi.org/10.1038/nmat4676.

[38] D.N. Micha, R.T. Silvares Junior, The influence of solar spectrum and concentration factor on the material choice and the efficiency of multijunction solar cells, Sci. Rep. 9 (1) (2019) 20055, http://dx.doi.org/10.1038/s41598-019-56457-0, Number: 1 Publisher: Nature Publishing Group.

[39] O. Dupré, R. Vaillon, M.A. Green, Physics of the temperature coefficients of solar cells, Sol. Energy Mater. Sol. Cells 140 (2015) 92–100, http://dx.doi.org/10.1016/j.solmat.2015.03.025.

[40] Z. Wang, H. Zhang, W. Zhao, Z. Zhou, M. Chen, The effect of concentrated light intensity on temperature coefficient of the InGaP/InGaAs/Ge triple-junction solar cell, Open Fuels Energy Sci. J. 8 (1) (2015).

[41] A. Riverola, A. Mellor, D.A. Alvarez, L.F. Llin, I. Guarracino, C.N. Markides, D.J. Paul, D. Chemisana, N. Ekins-Daukes, Mid-infrared emissivity of crystalline silicon solar cells, Sol. Energy Mater. Sol. Cells 174 (2018) 607–615.

[42] I.G. de Arrieta, T. Echániz, R. Fuente, G.A. López, Angle-resolved direct emissivity measurements on unencapsulated solar cells for passive thermal control, IEEE J. Photovolt. (2024).

[43] L. Micheli, K.S. Reddy, T.K. Mallick, Plate micro-fins in natural convection: An opportunity for passive concentrating photovoltaic cooling, Energy Procedia 82 (2015) 301–308, http://dx.doi.org/10.1016/j.egypro.2015.12.037.

[44] Manxuan Xiao, A review on recent development of cooling technologies for concentrated photovoltaics (CPV) systems, Energies (2018).